Supplementary Information A: Analytical mechanical modeling of nano-accordion structure

For analytical modeling one period of nano-accordion geometry is divided in three sections as shown in Fig. S1. Total strain in one period of nano-accordion structure is addition of strain due to unbending of curved section, stretching of ZnO-PDMS composite section and deflection of two vertical sections.

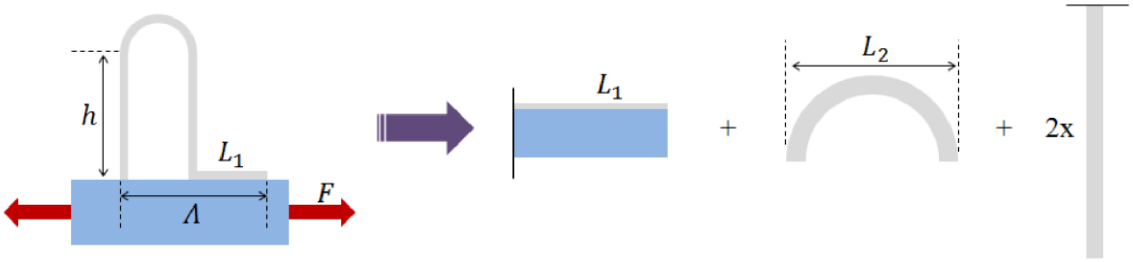

Figure S1. Division of one period of nano-accordion geometry in three parts

Strain in ZnO-PDMS composite section:

The schematic of ZnO-PDMS composite section is shown in Fig. S2. The length of the composite section is L_1 and, t_z and t_s are thicknesses of ZnO and PDMS substrate respectively. Both ZnO thin film and PDMS substrate has same width (b) along z-axis. Under applied external load F, the force component in ZnO thin film (P) is function of ZnO Young's modulus (E_z) and its cross-sectional area (A_z). Similarly, the force component in PDMS substrate is function of PDMS Young's modulus (E_s) and cross-sectional area (A_z). The external force F induces tensile stress in the composite section. The summation of forces along x-axis is given by, $F = P + P_s$. For a composite material under tensile loading, total strain is equal to strain in individual components. So the strain in ZnO thin film (ε_z) is equal to strain in PDMS substrate (ε_s), $\varepsilon_z = \varepsilon_s$, the forces can be expressed as $\frac{P}{A_z E_z} = \frac{P_s}{A_s E_s}$. Combining these results, the

force component in ZnO film is, $P = \frac{FA_zE_z}{A_zE_z+A_sE_s}$. The deformation of ZnO-PDMS composite due to stretching is then,

$$\delta_1 = \frac{PL_1}{A_zE_z} \tag{2}$$

This will be used to calculate the total deformation of the structure.

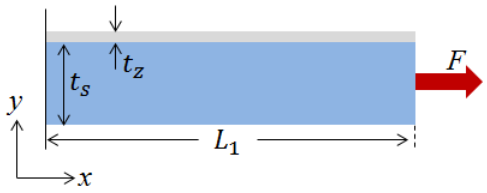

Figure S2. ZnO-PDMS composite section under tensile loading

Strain in curved section:

Under external loading, the curved section of nano-accordion behaves similar to unbending of a curved beam and is illustrated in Fig. S3. The curved section has a thickness t_z, inner radius r_1 and outer radius r_2. For bending of curved beams, the centroidal axis and neutral axis do not overlap and their radii are given by r_c and r_n respectively. The distance between two axes is given by, $e = r_c - r_n$. Given the nano-accordion has rectangular cross-section, the other radii of interests can be found to be $r_c = r_1 + \frac{t_z}{2}$ and $r_n = \frac{t_z}{\ln\left(\frac{r_2}{r_1}\right)}$ [1, 2].

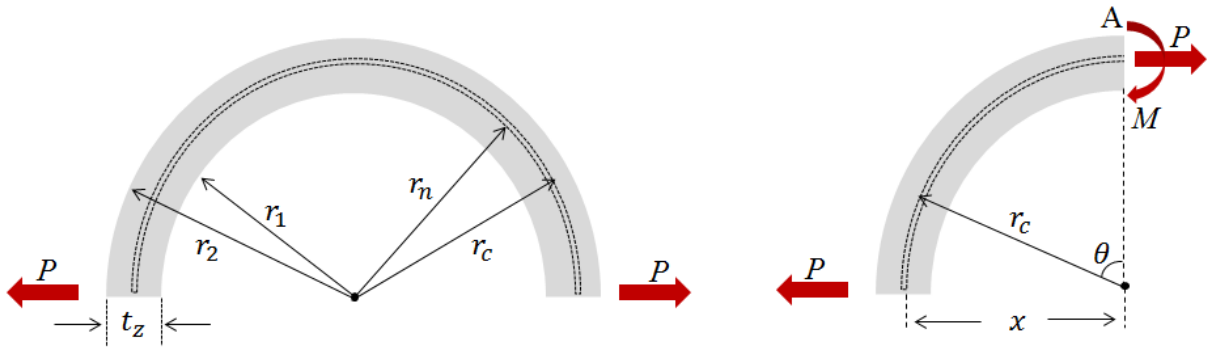

Figure S3. Curved section of nano-accordion under tensile loading

The strain induced in curved section due to external load F is dominated by bending moment M, which can be expressed as $M = Px = Pr_c\sin\theta$. Under external load the curved section undergoes deformation, and the strain energy (U) stored in this section in polar coordinate is given by, $U = \int_0^{\pi} \frac{M^2}{2EI} r_c d\theta = \frac{\pi P^2 r_c^3}{4EI}$, where, I is area moment of inertia for rectangular cross-section $I = \frac{bt_z^3}{12}$. Deflection of the curved section (δ_2) can be found by using Castigliano's theorem, $\delta_2 = \frac{dU}{dP}$, resulting in,

$$\delta_2 = \frac{6\pi P r_c^3}{bE_z t_z^3} \tag{3}$$

Deflection of vertical section:

Each period of nano-accordion consists of two vertical members and strain in this section is due to deflection under the applied load. This section behaves as cantilever beam under end load P.

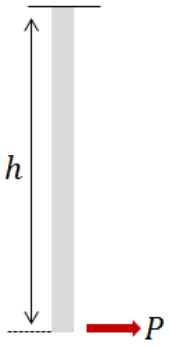

Figure S4. Deflection of vertical section of nano-accordion under loading

The deflection of cantilever beam under end load is given by, $\delta_3 = \frac{Ph^3}{3E_zI}$. Since each period has two vertical sections, the total deflection due to vertical section is,

$$\delta_3 = \frac{8Ph^3}{bE_z t_z^3} \tag{4}$$

The total deflection of the nano-accordion under external loading is obtained by adding the deflection of the three sections in equations (2), (3) and (4),

$$\delta_{total} = \delta_1 + \delta_2 + \delta_3 = \frac{P}{E_z b}\left(\frac{L_1}{t_z} + \frac{6\pi r_c^3}{t_z^3} + \frac{8h^3}{t_z^3}\right) \tag{5}$$

Upon examination, the deformations of curved and composite sections are negligible compared to the deflection of vertical section when *h* is large, the total strain simplifies to the following approximation,

$$\varepsilon_{total} = \frac{\delta_{total}}{\Lambda} = \frac{8Ph^3}{\Lambda E_z b t_z^3} \tag{6}$$

Here we can observe that the total strain is related to the internal force *P* and other geometric and material parameters. The next step is to derive the stress on the curve section, which is believed to undergo the highest local stress within the structure. The maximum tensile stress (σ)

appearing on the inner edge of curved section and is given by, $\sigma = \frac{Mt_z}{2A_z e r_1} = \frac{Pr_c}{2ber_1}$. To simplify the analysis using a first-order approximation, the curved section assumed to be a straight beam. The maximum stress due to bending moment is given by, $\sigma = \frac{Mt_z}{2I} = \frac{6\mathrm{Pr}_2}{bt_z^2}$. For small thickness of nano-accordion $t_z \to 0$, $r_2 \approx r_c$, yielding $\sigma = \frac{6\mathrm{Pr_c}}{bt_z^2}$. The internal force can then be represented as a function of maximum stress $P = \frac{\sigma_1 bt_z^2}{6r_c}$, resulting in,

$$\varepsilon_{total} = \frac{4\sigma}{3\Lambda E_z r_c}\left(\frac{h^3}{t_z}\right) \tag{7}$$

This equation describes the total structure strain as a function of the maximum stress, which is located at in the curved section. Setting the stress to be σ_{FS}, the maximum strain can be defined to be a function of geometric parameters, and scales linearly with the parameter h^3/t_z. This result provides the scaling law and guiding principle on designing the stretchability of the nano-accordion structure.

Uniaxial tensile test in SEM:

The uniaxial tensile tests are carried out on the nano-accordion samples, and the corresponding change in the periodicity of nano-accordion structure is recorded by observing the sample under SEM. Figure S5 shows the tensile testing stage with 30 nm nano-accordion sample at 0% strain. After mounting the sample on stage, it is loaded in SEM and nano-accordion period is recorded at 0% strain. The stage is then removed from SEM chamber and sample is then stretched to desired strain, before confirming the strain by measuring the resulting period changes. The samples are tested by cycles of loading and unloading of sample within SEM chamber to determine the maximum strain that the nano-accordion structure can withstand under tensile loading.

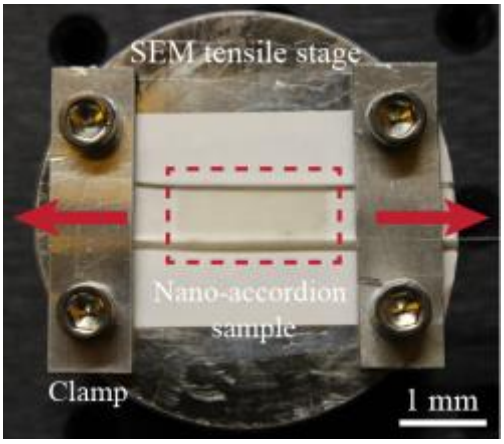

Figure S5. SEM tensile test stage with 30 nm nano-accordion sample at 0% strain. Red arrows indicate the direction of stretching.

Figure S6 shows the SEM image of 30 nm planer ZnO film on PDMS substrate after lift-off process with 0% strain. The SEM image shows that the film has developed numerous cracks during transfer to PDMS substrate and during careful handling of sample for SEM imaging. This indicates that, the 30 nm planer ZnO film is very brittle and cracks readily through handling, making it unsuitable for applications involving stretching and/or bending.

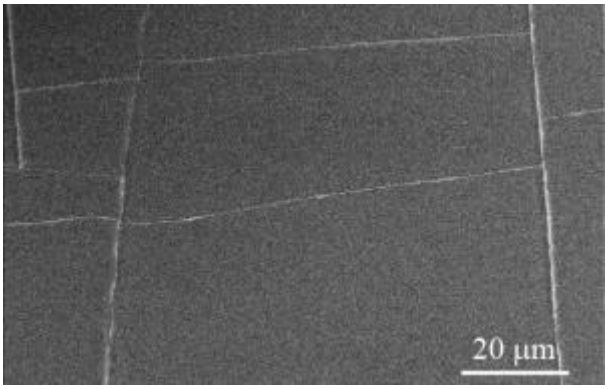

Figure S6. SEM image of 30 nm planar ZnO film on PDMS substrate after lift-off.

Supplementary Information B: Compression induced breaking of nano-accordion structure

When nano-accordion structure is stretched, it experiences tensile stress in the fold direction of the nano-accordion geometry and compressive stress along ridge direction. Tensile stress results in stretching of the sample, facilitated by increase in period of fold geometry. But due to the 1D nature of fold geometry, compressive stress in the ridge direction results in buckling of the sample. Compression induced failures for 30 nm, 50 nm, and 70 nm thick nano-accordion structures at constant height and period are shown in Fig. S7a – c, respectively. For these three samples the initial compression induced failure was observed for strain values between 10% - 15%, which is less than the failure strain to induce systematic failure along the fold direction. These failures occur due to inherent 1D nature of the accordion geometry, and can be mitigated by using 2D fold structures. This will be explored in future work.

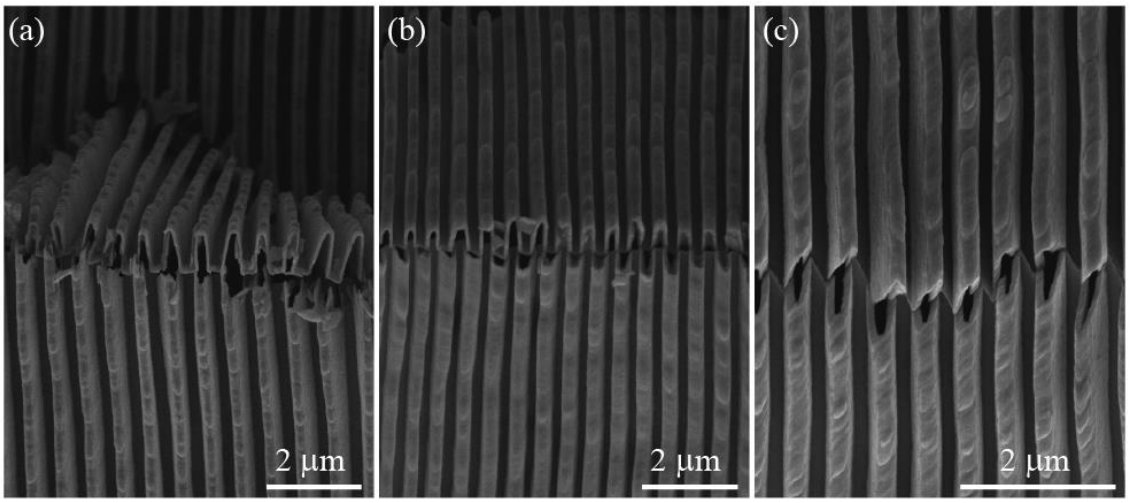

Figure S7. Top-view SEM images showing systematic failure of nano-accordion structure due to compressive loading in the ridge direction. The fabricated structures have 1100 nm height, 500nm period and ZnO film with different thicknesses. (a) t_z = 30 nm, (b) t_z = 50 nm, (c) t_z = 70 nm

Supplementary Information C: FEA model and further mechanical analysis

The effect of film thickness on stretchability of nano-accordion geometry is also studied. Three samples with thicknesses 30 nm, 50 nm and 70 nm are tested and the failure strain are found to be 53%, 33%, and 21%, respectively, for a constant structure height of 1100 nm and period 500 nm. The stretchability of nano-accordion geometry decreases with increase in thickness. From SEM images in Fig S8a – c, it is observed that at maximum failure strain, crack appears on top of the nano-accordion structure and propagates along ridge direction. This failure behavior indicates that under tensile loading, maximum stress occurs in the curved section of nano-accordion structure leading to formation and subsequent propagation of crack.

This hypothesis is verified using finite element model for a nano-accordion structure with h = 1100 nm, t_z = 30 nm, Λ = 500 nm, and r_2 = 115 nm is shown in Fig. S8d. In this model the top curvy section of nano-accordion structure as seen from SEM images is approximated as perfect semi-circle with diameter equal to the structure width. A 2D model (plane strain) with infinite depth is assumed, and the Young's modulus (E_z) and Poison's ratio (ν_z) used for numerical analysis of ZnO are 129 GPa and 0.349 [3] respectively. The simulated stress contours with 53% strain is depicted in Fig. S6d and the maximum stress of 757 MPa can be observed at the inner curved sections. It is important to note that as a result of the nano-accordion geometry, the local stress is much lower in contrast to the case where a planar film is subjected to the same strain. At 53% strain the stress in this section is about 757 MPa, indicating this to failure stress for 30 nm thick ZnO nano-accordion structure. This stress concentration is the result of unbending of curved section caused by stretching of nano-accordion structure. The stress profile along the curve sections indicates tensile stress at the inner and compressive stress at the outer portion, which is characteristic of bending. FEA models of other structure height and thickness

combinations also resulted in similar stress profiles showing stress concentration in the inner curved section.

The FEA model also validates that the maximum contribution to strain originates from the deflection of vertical sections in the nano-accordion geometry, as expected. Taller and thinner nano-accordion structures have lower stiffness, resulting in better stretchability. This observation is in line with the experimental results. From these experiments it is clear that mechanical characteristics of stretchable nano-accordion structure are function of its geometrical parameters. These geometrical parameters can easily be controlled using the fabrication technique proposed in this work to achieve specific mechanical performance.

Maximum stress vs strain curves plotted using FEA model for 1100 nm tall ZnO nano-accordion structures with different film thicknesses are shown in Fig. S8e. The maximum failure strain values for these samples, known from experimental results, are plotted on these curves to get the corresponding failure stress. From experimental and FEA results it is observed that, increasing the structure thickness results in higher resistance to the bending mode, thereby increasing the stress concentration and lowering the stretchability. The black dotted line represents averaged failure stress value for these samples, which is about 800 MPa. The averaged failure stress value for these set of samples too is close to 800 MPa. This is similar in magnitude but higher than tensile strength value for sputtered ZnO of 412 ± 50 MPa reported in literature [4], which could be attributed to more robust ZnO film deposited by ALD process.

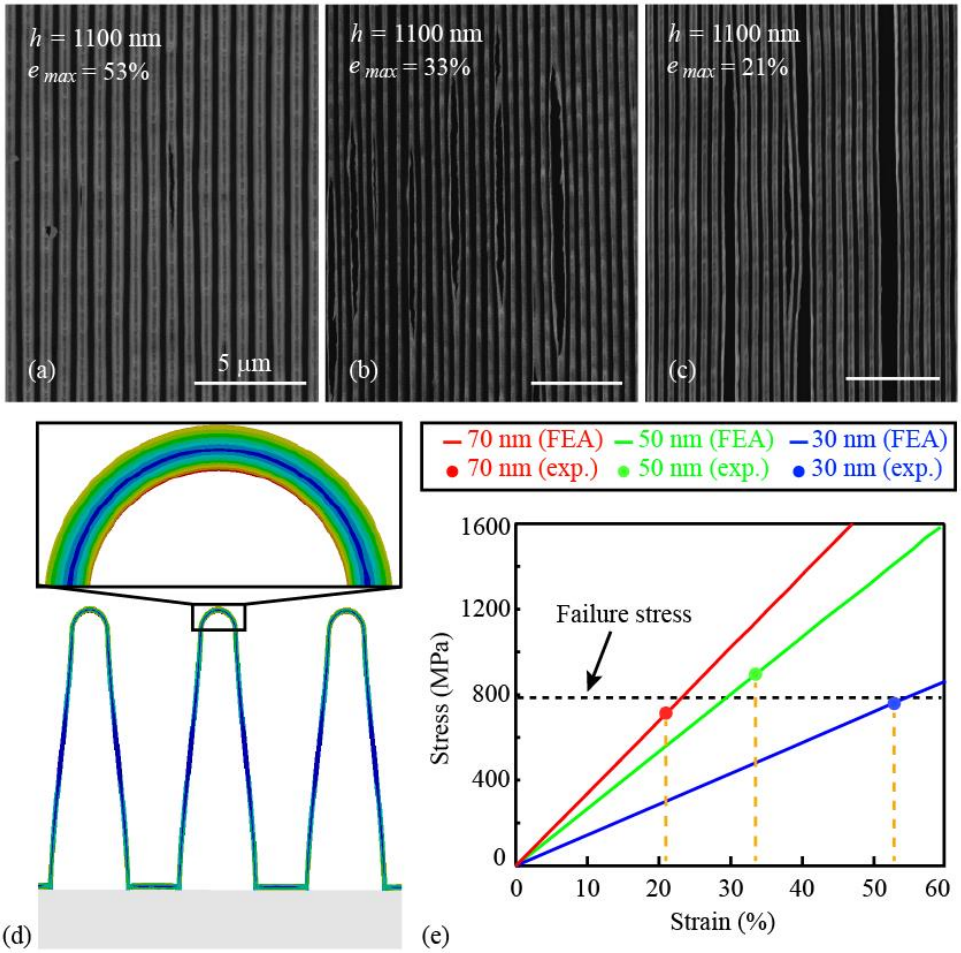

Figure S8. Top-view SEM images showing systematic failure of nano-accordion structure along the grating direction. The fabricated structures have 1100 nm height, 500nm period and ZnO film with different thicknesses. (a) t_z = 30 nm, ϵ_{max} = 53% (b) t_z = 50 nm, ϵ_{max} = 33% (c) t_z = 70 nm, ϵ_{max} = 21%. (d) FEA model showing highest stress in the inner curved section of nano-accordion geometry under tensile loading. Failure stress (red) is about 760 MPa for a sample with h = 1100 nm, t_z = 30 nm, Λ = 500 nm, and r_2 = 115 nm. (e) Simulated stress vs strain curve for h = 1100 nm and Λ = 500 nm, with different thicknesses. Experimental results for failure strain are plotted on respective curves to get corresponding local stress. Black dotted line indicates averaged failure stress, which is about 800 MPa.

From the analytical model presented in equation (7), the stretchability of nano-accordion structure has cubic relationship with the nano-accordion height. The predicted stretchability values *vs* nano-accordion height for structures with thicknesses of 30, 50, and 70 nm are plotted in Fig. S9. The experimental data and corresponding FEA results are also plotted, exhibiting the

cubic relationship predicted by the analytical model. The experimental and FEA results match closely with the analytical model.

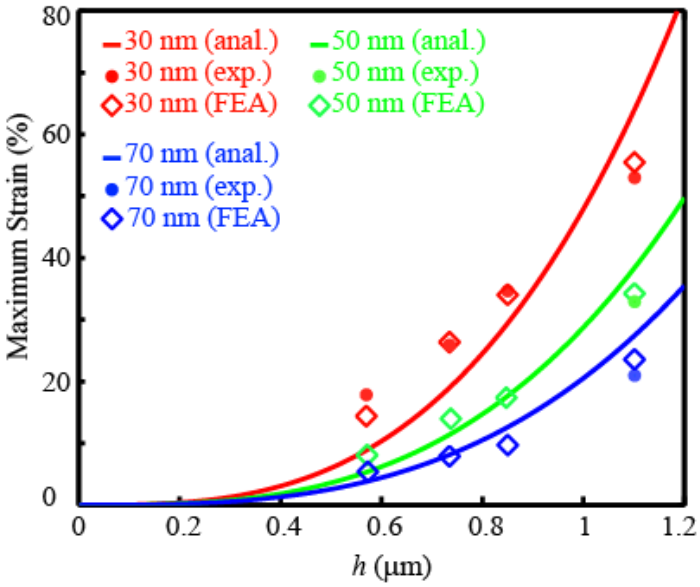

Figure S9. Comparison of stretchability versus nano-accordion height using the analytical model, FEA, and experimental data.

Supplementary Information D: Electrical properties of Al doped ZnO

To further enhance the functionality of the nano-accordion structure, the deposited film can be doped to be conductive during ALD process. Addition of Al leads to Zn^{2+} ion in ZnO wurtzite crystal structure being replaced by Al^{3+} ion, generating a free electron in conduction band to increase the n-type electrical conductivity [5]. The AZO films are deposited with 13:1 ratio for ZnO and Al_2O_3, their mechanical properties will be similar to that of ZnO. Using AZO as the film material, the nano-accordion structure is simultaneously stretchable, transparent, and conductive. Electrical characterization is carried out by applying a fixed voltage across sample and measuring the current at various uniaxial tensile strain values to calculate corresponding resistance of the sample.

AZO film thickness (nm)	Resistivity of flat AZO (Ω·cm)	Resistivity before lift-off (Ω·cm)	Resistivity after lift-off (Ω·cm)
30	2.407	3.233	13.086
50	0.186	0.220	0.751
70	0.032	0.036	0.259

Resistivity of AZO nano-accordion film before lift-off in solvent solution is slightly higher than the resistivity of flat AZO film, for all thicknesses. This could be attributed to the lower effective mean free path of electrons in the nano-accordion film compared to the flat film, resulting from higher surface roughness than planer film [6], and fold geometry. Though nano-accordion structure with 30 nm AZO thickness will be highly stretchable, 50 nm AZO thickness is used to improve electrical properties resulting from higher number of charge carriers. The nano-accordion structure is anisotropic and has different electrical properties along fold direction and ridge direction. The electrical properties reported here are in the fold direction of nano-accordion

geometry. The measured resistivity of the nano-accordion structure on PDMS substrate with 30, 50, and 70 nm thicknesses without strain are 13.086 Ω-cm, 0.751 Ω-cm, and 0.259 Ω-cm respectively, where the total length of the nanostructure along the fold direction is used. However, the resistivity of the 50 nm-thick AZO nano-accordion structure immediately after deposition is 0.22 Ω-cm. The cause of degradation in electrical property during the lift-off process is not well understood, and is the subject of future studies.

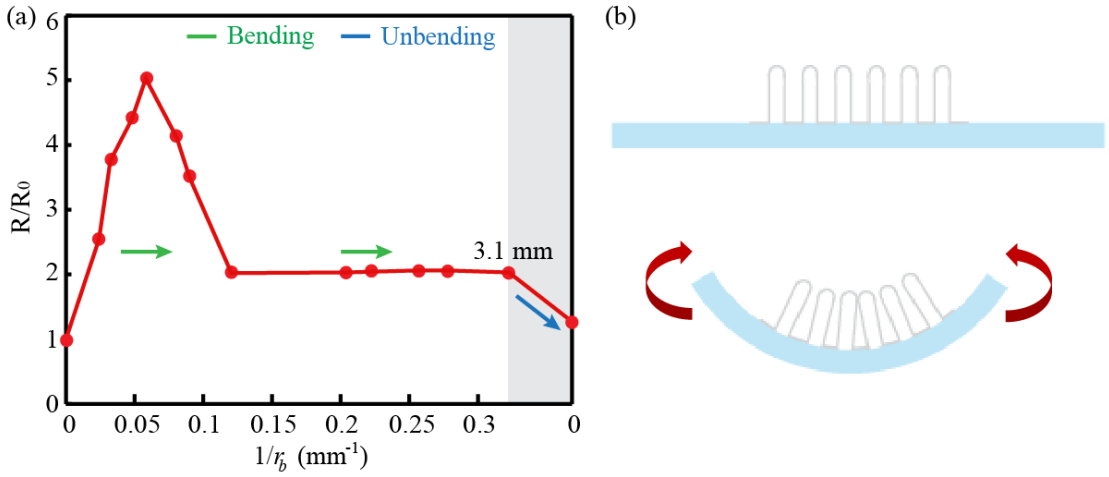

Figure S10. (a) Relative resistance versus bending radius. (b) Schematic of bending mechanism

Electrical performance of the 50 nm AZO nano-accordion structure on PDMS is also tested when it is bent such that during bending, the nano-accordion structure is under compressive loading. The relative resistance of the structure starts to increase as soon as the bending starts, reaching to 5 times of initial value at a bend radius of about 11 mm, as shown in Fig. S10a. As the bend radius is further reduced, the normalized resistance starts to decrease gradually and reaches to 2 times of initial value at a bend radius of 4.9 mm. This phenomenon could be attributed to curved sections of nano-accordion structure coming together under bending as illustrated in Fig. S10b. The relative resistance remains constant for further increase in bend radius, indicating that no

substantial damage is caused by contact made between adjacent nano-accordion structures. The relative resistance is recovered to 1.24 times of initial value when unbent.

Supplementary Information E: Optical simulation of nano-accordion structure

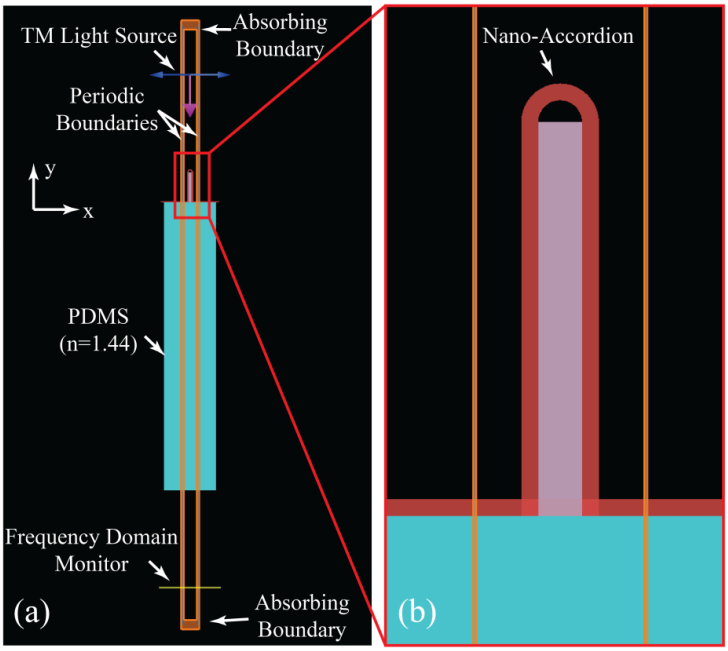

Figure S11. (a) 2D simulation setup. (b) Magnified view of nano-accordion structure.

The optical simulation was conducted using Lumerical's FDTD Solutions 8.9. The simulation setup is shown in Fig. S11. One cell of nano-accordion structure was constructed in 2D with periodic boundary conditions along x direction and absorbing boundary conditions along y direction, as depicted in Fig. S11a. The structures were normally illuminated by a pulsed light source for spectral analysis. The PDMS layer was set to be 10 μm thick and the frequency domain intensity monitor was 3 μm away from the PDMS bottom interface for coherent transverse-electric (TE) and transverse-magnetic (TM) illuminations. The unpolarized transmission spectra were calculated by averaging TE and TM results. In the simulations, PDMS was assumed non-dispersive with refractive index of 1.44 and the nanostructure material was set to ZnO with dispersion relation obtained by ellipsometric measurement of a planar ZnO film deposited by atomic layer deposition (ALD). The incoherent results were obtained using equation (8) where a Lorentzian weighting function with optimal coherence length of 5.5 μm was

used for spectral averaging of the coherent results to imitate the light source in the spectrophotometer (Agilent Cary 5000 UV-Vis-NIR).

$$I'(\omega_0) = \int \frac{\delta}{(\omega - \omega_0)^2 + (\pi\delta)^2} I(\omega) d\omega \tag{8}$$

Where $I(\omega)$ and $I'(\omega_0)$ are the coherent and incoherent intensity spectra as a function of angular frequency, respectively. And $\delta = l_c/c$, where l_c is coherence length and c is speed of light.

Supplementary Information F: Birefringence and light trapping effect of nano-accordion structure

Experimental broadband optical transmittance spectra of 30 nm AZO film on glass slide for unpolarized light is plotted in Fig. S12. For 30 nm AZO film sample, the transmittance drops over visible spectrum to 80% at 400 nm wavelength. The AZO film deposited by ALD process has low surface roughness so the diffused portion of light transmitted through this sample is almost zero.

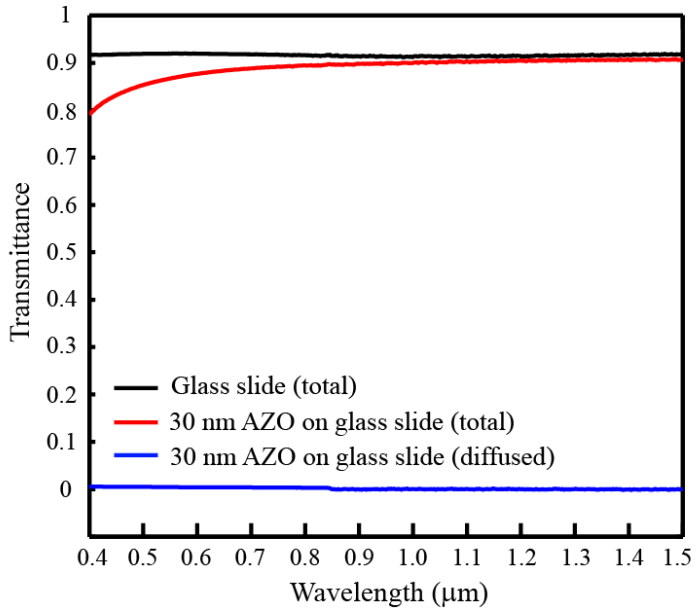

Figure S12. Broadband optical transmittance spectra of 30 nm AZO film on glass slide

Experimental and simulated broadband optical transmittance spectra for 30 nm, 50 nm, and 70 nm AZO thicknesses for TE and TM mode are plotted in Fig. S13a - b. It can be observed that for both TE and TM mode the transmittance is inversely related to the AZO film thickness. For all samples, over visible spectrum, TE mode has lower transmittance compared to TM mode. This difference in transmittance spectra for TE and TM mode is due to form birefringence

resulting from nano-accordion structure geometry. The birefringence phenomenon is not strong, but can be visually observed for 50 nm AZO nano-accordion sample is shown in Fig. S13c. This structure induced birefringence is observed only along fold direction of nano-accordion geometry and can lead to interesting polarization sensitive devices.

Under normal incidence of light on nano-accordion structure, the higher diffracted orders get trapped in PDMS due to total internal reflection. This can also be observed in Fig. S13d, where bright PDMS edge indicates trapped light coming out through the edge of PDMS. This loss due to diffracted orders trapped in PDMS results in lower transmittance and can be overcome by designing nano-accordion structures with subwavelength period.

Figure S13e shows the total, specular and diffused transmission for 70 nm AZO nano-accordion structure on PDMS substrate. The diffused transmission for 70 nm AZO nano-accordion film is about 4% over visible spectrum, which is higher compared to the flat AZO film of same thickness. The higher diffused transmission could have resulted from scattering due to line-edge roughness (LER). The fabricated nano-accordion structures have line-edge roughness along ridge direction resulting from under-exposed photoresist template during interference lithography. The photoresist template is under-exposed to facilitate lift-off off ZnO/AZO nano-accordion structure on PDMS substrate. The line-edge roughness can be overcome by avoiding under-exposure of photoresist and using some sacrificial layer to facilitate lift-off process.

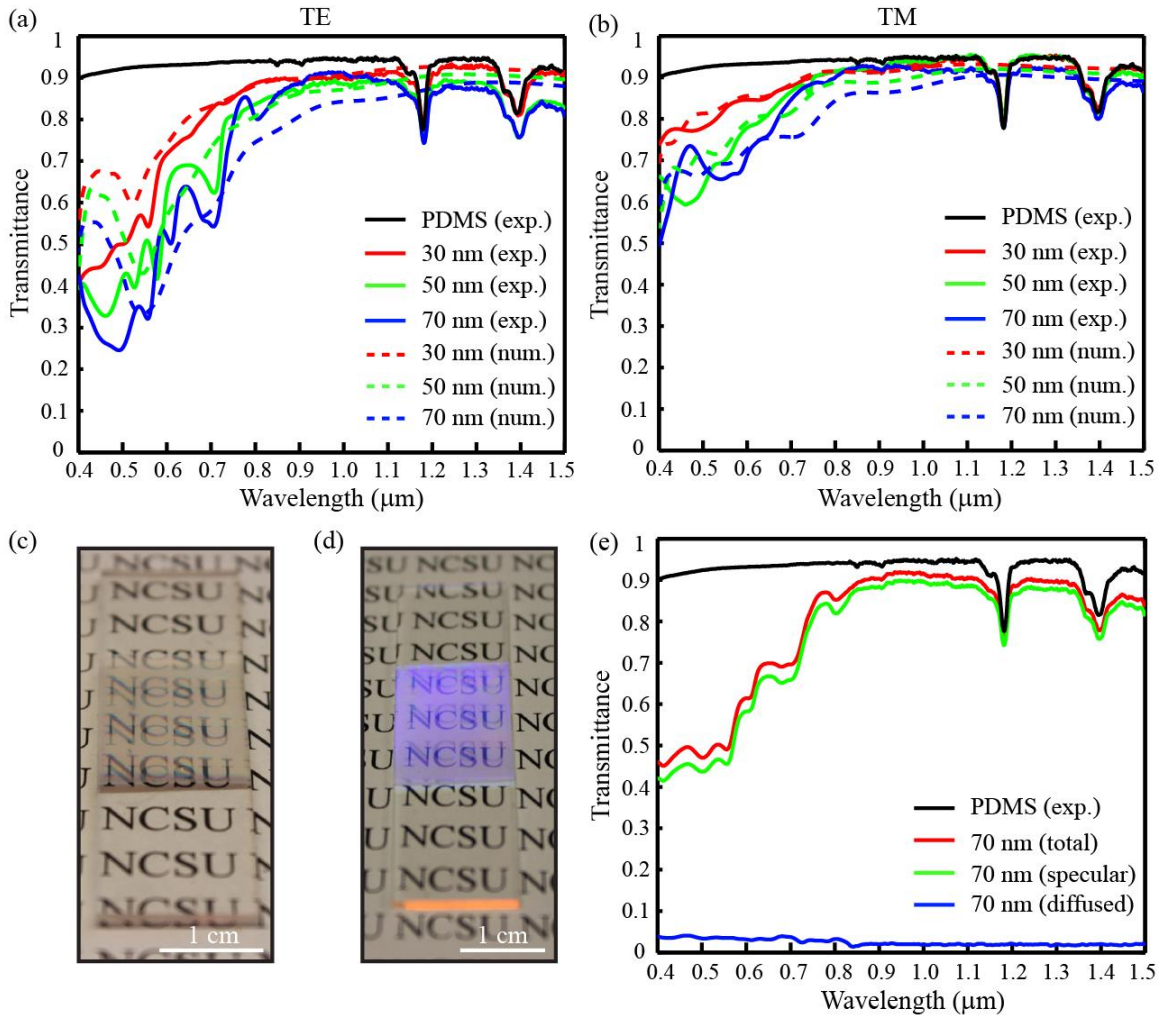

Figure S13. (a) TE and, (b) TM broadband optical transmittance of 30, 50, and 70 nm nano-accordion structure on PDMS. (c) Birefringence effect of nano-accordion structure. Optical image of 50 nm AZO nano-accordion structure on PDMS. The structure exhibits directional birefringence along fold direction of nano-accordion geometry. (d) Diffraction and light trapping effect of nano-accordion structure. Optical image of 50 nm AZO nano-accordion structure on PDMS under normal incidence of white light. Bright orange color at the edge of PDMS is due to diffracted orders trapped in PDMS. (e) Total, specular and diffused transmission for 70 nm AZO nano-accordion structure on PDMS.

References:

1. Beer, F. P., Johnston, E. R. Jr., DeWolf, J. T., Mazurek, D. F. *Mechanics of Materials*. McGraw Hill, New York, New York, sixth edition, **2012**.
2. Budynas, R. G., Nisbett, J. K. *Shigley's Mechanical Engineering Design*. McGraw Hill, New York, New York, eighth edition, **2008**.
3. Gao, Y.; Wang, Z. L. Equilibrium Potential of Free Charge Carriers in a Bent Piezoelectric Semiconductive Nanowire. *Nano Lett.* **2009**, *9*, 1103–1110.
4. Ong, C. W.; Zong, D. G.; Aravind, M.; Choy, C. L.; Lu, D. R. Tensile Strength of Zinc Oxide Films Measured by a Microbridge Method. *Journal of Materials Research* **2003**, *18*, 2464–2472.
5. Maldonado, F.; Stashans, A. Al-Doped ZnO: Electronic, Electrical and Structural Properties. *Journal of Physics and Chemistry of Solids* **2010**, *71*, 784–787.
6. Marom, H.; Eizenberg, M. The Effect of Surface Roughness on the Resistivity Increase in Nanometric Dimensions. *Journal of Applied Physics* **2006**, *99*, 123705.